Metal-coated magnetic nanoparticles in an optically active medium: A nonreciprocal metamaterial

Aristi Christofi* and Nikolaos Stefanou
Department of Solid State Physics, National and Kapodistrian University of Athens, Panepistimioupolis, GR-157 84 Athens, Greece

(Received 7 February 2018; published 16 March 2018)

We report on the optical response of a nonreciprocal bianisotropic metamaterial, consisting of spherical, metal-coated magnetic nanoparticles embedded in an optically active medium, thus combining gyrotropy, plasmonic resonances, and chirality in a versatile design. The corresponding effective medium is deduced by an appropriate two-step generalized Maxwell-Garnett homogenization scheme. The associated photonic band structure and transmission spectra are obtained through a six-vector formulation of Maxwell equations, which provides an efficient framework for general bianisotropic structures going beyond existing approaches that involve cumbersome nonlinear eigenvalue problems. Our results, analyzed and discussed in the light of group theory, provide evidence that the proposed metamaterial exhibits some remarkable frequency-tunable properties, such as strong, plasmon-enhanced nonreciprocal polarization azimuth rotation and magnetochiral dichroism.

DOI: 10.1103/PhysRevB.97.125129

I. INTRODUCTION

The interaction of optical fields with magnetic materials breaks local time-reversal symmetry, providing a versatile route for designing nonreciprocal photonic components based, e.g., on the Faraday rotation effect. In particular, with the incorporation of metallic nanostructures that support localized plasmon modes, the inherently weak magneto-optical coupling at visible and near-infrared frequencies can be greatly enhanced in subwavelength volumes, thus allowing for the realization of ultracompact magneto-optical devices [1–5]. However, spectral nonreciprocity is, in principle, encountered in systems which lack both time-reversal and space-inversion symmetries [6], and various designs of macroscopic magnetophotonic structures without an inversion center have been proposed and elaborated for this purpose [7–10]. Space-inversion symmetry can also be removed by the presence of inherently optically active materials or substances, due to a chiral arrangement of their atomic/molecular constituents or an inherent chiral structure of their molecules themselves, and composite structures with such optically active components are promising candidates for exotic optical functions as in photonic band engineering [11–13], nonlinear optics [14], and negative refraction [15].

In the present paper, we seek to combine magnetic functionalities, plasmonic resonances, and chirality in a versatile system consisting of an assembly of metal-coated magnetic nanoparticles immersed in an optically active medium. Magnetic properties are exhibited by the core material, the metallic shell introduces plasmonic resonances, while chirality is provided by the host. This composite medium can be treated as an optically uniform metamaterial in the visible and near-infrared parts of the spectrum since the wavelength is much longer than the size of the particles and the distances between them, and exhibits an intriguing nonreciprocal optical response. The remainder of the paper is organized as follows: In Sec. II, we develop a versatile six-vector formalism for calculating the eigenmodes of the electromagnetic (EM) field in a homogeneous, in general bianisotropic, medium as well as the transmission, reflection, and absorption coefficients of layered structures of such media. Moreover, we report closed-form expressions for the homogenization of the composite medium under consideration using a two-step Maxwell-Garnett effective-medium approximation. In Sec. III, we undertake a comprehensive analysis of the photonic dispersion diagram of the given metamaterial, in conjunction with associated transmission spectra, and discuss some remarkable nonreciprocal effects, namely, polarization azimuth rotation and magnetochiral dichroism. Our results are summarized in Sec. IV.

II. THEORY

A. Electromagnetic waves in bianisotropic media

In the class of materials that go under the generic name of bianisotropic materials, the linear response to EM fields is described by the phenomenological constitutive relations

$$\begin{pmatrix} \frac{1}{\epsilon_0}\mathbf{D} \\ \frac{1}{\sqrt{\epsilon_0\mu_0}}\mathbf{B} \end{pmatrix} = \begin{pmatrix} \boldsymbol{\epsilon} & \boldsymbol{\xi} \\ \boldsymbol{\zeta} & \boldsymbol{\mu} \end{pmatrix} \begin{pmatrix} \mathbf{E} \\ \sqrt{\frac{\mu_0}{\epsilon_0}}\mathbf{H} \end{pmatrix} \equiv \mathbf{M} \begin{pmatrix} \mathbf{E} \\ \sqrt{\frac{\mu_0}{\epsilon_0}}\mathbf{H} \end{pmatrix} \quad (1)$$

between the electric and magnetic fields, $\mathbf{E}$ (in V/m) and $\mathbf{H}$ (in A/m), and the electric and magnetic flux densities, $\mathbf{D}$ (in $\mathrm{C/m^2}$) and $\mathbf{B}$ (in $\mathrm{Wb/m^2}$), where ϵ_0 and μ_0 are the vacuum electric permittivity and magnetic permeability, respectively. $\mathbf{M}$ is defined as a 6×6 dimensionless matrix, which contains the relative electric permittivity $\boldsymbol{\epsilon}$, magnetic permeability $\boldsymbol{\mu}$, and magnetoelectric cross-coupling $\boldsymbol{\xi}$ and $\boldsymbol{\zeta}$ tensors. The latter are nonzero, e.g., for optically active chiral media, as we shall see below. Maxwell equations for EM fields with $\exp(-i\omega t)$ harmonic time dependence in such a medium can be cast in the form of a generalized eigenvalue problem,

$$\begin{pmatrix} \mathbf{0} & -\boldsymbol{\nabla}\times \\ \boldsymbol{\nabla}\times & \mathbf{0} \end{pmatrix} \begin{pmatrix} \mathbf{E} \\ Z\mathbf{H} \end{pmatrix} = \frac{i\omega}{c} \begin{pmatrix} \boldsymbol{\epsilon} & \boldsymbol{\xi} \\ \boldsymbol{\zeta} & \boldsymbol{\mu} \end{pmatrix} \begin{pmatrix} \mathbf{E} \\ Z\mathbf{H} \end{pmatrix}, \quad (2)$$

*aristi.christofi@gmail.com

where $Z = \sqrt{\mu_0/\epsilon_0}$ and $c = 1/\sqrt{\epsilon_0\mu_0}$ are the vacuum wave impedance and velocity, respectively. We note that for $\omega \neq 0$, the divergence Maxwell equations are automatically satisfied [16].

Seeking solutions of Eq. (2) in the form of plane waves, $\mathbf{E}(\mathbf{r}) = \mathbf{E}_0 \exp(i\mathbf{q}\cdot\mathbf{r})$, $\mathbf{H}(\mathbf{r}) = \mathbf{H}_0 \exp(i\mathbf{q}\cdot\mathbf{r})$, with given x and y components of wave vector $\mathbf{q}$, leads to the following eigenvalue-eigenvector equation for the q_z component and the corresponding polarization eigenvectors $\widehat{\mathbf{e}} = \mathbf{E}_0/E_0$, $\mathbf{h} = Z\mathbf{H}_0/E_0$, where $E_0 = |\mathbf{E}_0|$,

$$\left[\frac{\omega}{c}\begin{pmatrix}\boldsymbol{\epsilon} & \boldsymbol{\xi}\\ \boldsymbol{\zeta} & \boldsymbol{\mu}\end{pmatrix} + \begin{pmatrix}\mathbf{0} & \mathbf{C}_1\\ -\mathbf{C}_1 & \mathbf{0}\end{pmatrix}\right]^{-1}\begin{pmatrix}\mathbf{0} & \mathbf{C}_2\\ -\mathbf{C}_2 & \mathbf{0}\end{pmatrix}\begin{pmatrix}\widehat{\mathbf{e}}\\ \mathbf{h}\end{pmatrix} = \frac{1}{q_z}\begin{pmatrix}\widehat{\mathbf{e}}\\ \mathbf{h}\end{pmatrix}, \tag{3}$$

where

$$\mathbf{C}_1 = \begin{pmatrix}0 & 0 & q_y\\ 0 & 0 & -q_x\\ -q_y & q_x & 0\end{pmatrix},\quad \mathbf{C}_2 = \begin{pmatrix}0 & 1 & 0\\ -1 & 0 & 0\\ 0 & 0 & 0\end{pmatrix}. \tag{4}$$

The above 6×6 linear eigenvalue problem can be solved by standard numerical algorithms [17], which are much faster than quadradic eigenvalue solvers [18,19] as required in alternative 3×3 matrix formulations of Maxwell equations [5]. We denote the four physically acceptable (nonzero eigenvalue) solutions of Eq. (3) by a superscript $s = +(-)$, which corresponds to waves propagating or decaying in the positive (negative) z direction, and a subscript $p = 1,2$, which labels the two linearly independent polarization eigenmodes. The electric and magnetic field components of these waves, with wave vector $\mathbf{q}_p^s = \mathbf{q}_\parallel + q_{z;p}^s\widehat{\mathbf{z}}$ and polarization eigenvectors $\widehat{\mathbf{e}}(\mathbf{q}_p^s)$ and $\mathbf{h}(\mathbf{q}_p^s)$, are given by

$$\mathbf{E}(\mathbf{r},t) = \mathrm{Re}\{E_0\exp[i(\mathbf{q}_p^s\cdot\mathbf{r}-\omega t)]\widehat{\mathbf{e}}(\mathbf{q}_p^s)\},$$
$$\mathbf{H}(\mathbf{r},t) = \frac{1}{Z}\mathrm{Re}\{E_0\exp[i(\mathbf{q}_p^s\cdot\mathbf{r}-\omega t)]\mathbf{h}(\mathbf{q}_p^s)\}. \tag{5}$$

We now consider a planar interface between two different homogeneous, in general bianisotropic, media: (1) on the left and (2) on the right of the interface. We assume that the interface is perpendicular to the z axis, which is directed from left to right, at $z = 0$. Let us consider a plane EM wave of amplitude E_{in}, angular frequency ω, wave vector $\mathbf{q}_{p'}^{+(1)}$ and polarization eigenvectors $\widehat{\mathbf{e}}(\mathbf{q}_{p'}^{+(1)})$, $\mathbf{h}(\mathbf{q}_{p'}^{+(1)})$, incident on the interface from the left. Scattering at the interface gives rise to reflected and transmitted plane waves of wave vectors $\mathbf{q}_p^{-(1)}$ and $\mathbf{q}_p^{+(2)}$, $p = 1,2$, respectively, and associated polarization eigenvectors. Time invariance and translation invariance parallel to the interface imply that ω and $\mathbf{q}_\parallel$ remain the same for all of these waves, while linearity imposes that the corresponding amplitudes are proportional to E_{in}. Let us write them as $S_{pp'}^{-+}E_{\mathrm{in}}$ and $S_{pp'}^{++}E_{\mathrm{in}}$, respectively. Continuity of the tangential components of the wave field at the interface yields

$$\begin{pmatrix}-\widehat{e}_x(\mathbf{q}_1^{-(1)}) & -\widehat{e}_x(\mathbf{q}_2^{-(1)}) & \widehat{e}_x(\mathbf{q}_1^{+(2)}) & \widehat{e}_x(\mathbf{q}_2^{+(2)})\\ -\widehat{e}_y(\mathbf{q}_1^{-(1)}) & -\widehat{e}_y(\mathbf{q}_2^{-(1)}) & \widehat{e}_y(\mathbf{q}_1^{+(2)}) & \widehat{e}_y(\mathbf{q}_2^{+(2)})\\ -h_x(\mathbf{q}_1^{-(1)}) & -h_x(\mathbf{q}_2^{-(1)}) & h_x(\mathbf{q}_1^{+(2)}) & h_x(\mathbf{q}_2^{+(2)})\\ -h_y(\mathbf{q}_1^{-(1)}) & -h_y(\mathbf{q}_2^{-(1)}) & h_y(\mathbf{q}_1^{+(2)}) & h_y(\mathbf{q}_2^{+(2)})\end{pmatrix}\begin{pmatrix}S_{1p'}^{-+}\\ S_{2p'}^{-+}\\ S_{1p'}^{++}\\ S_{2p'}^{++}\end{pmatrix} = \begin{pmatrix}\widehat{e}_x(\mathbf{q}_{p'}^{+(1)})\\ \widehat{e}_y(\mathbf{q}_{p'}^{+(1)})\\ h_x(\mathbf{q}_{p'}^{+(1)})\\ h_y(\mathbf{q}_{p'}^{+(1)})\end{pmatrix}, \tag{6}$$

for $p' = 1,2$. Similarly, for incidence on the interface from the right, we obtain the corresponding reflection and transmission amplitudes, $S_{pp'}^{+-}$ and $S_{pp'}^{--}$, respectively, from the linear system,

$$\begin{pmatrix}-\widehat{e}_x(\mathbf{q}_1^{-(1)}) & -\widehat{e}_x(\mathbf{q}_2^{-(1)}) & \widehat{e}_x(\mathbf{q}_1^{+(2)}) & \widehat{e}_x(\mathbf{q}_2^{+(2)})\\ -\widehat{e}_y(\mathbf{q}_1^{-(1)}) & -\widehat{e}_y(\mathbf{q}_2^{-(1)}) & \widehat{e}_y(\mathbf{q}_1^{+(2)}) & \widehat{e}_y(\mathbf{q}_2^{+(2)})\\ -h_x(\mathbf{q}_1^{-(1)}) & -h_x(\mathbf{q}_2^{-(1)}) & h_x(\mathbf{q}_1^{+(2)}) & h_x(\mathbf{q}_2^{+(2)})\\ -h_y(\mathbf{q}_1^{-(1)}) & -h_y(\mathbf{q}_2^{-(1)}) & h_y(\mathbf{q}_1^{+(2)}) & h_y(\mathbf{q}_2^{+(2)})\end{pmatrix}\begin{pmatrix}S_{1p'}^{--}\\ S_{2p'}^{--}\\ S_{1p'}^{+-}\\ S_{2p'}^{+-}\end{pmatrix} = -\begin{pmatrix}\widehat{e}_x(\mathbf{q}_{p'}^{-(2)})\\ \widehat{e}_y(\mathbf{q}_{p'}^{-(2)})\\ h_x(\mathbf{q}_{p'}^{-(2)})\\ h_y(\mathbf{q}_{p'}^{-(2)})\end{pmatrix}, \tag{7}$$

for $p' = 1,2$. We note that the 4×4 matrices on the left-hand side of Eqs. (6) and (7) are identical, so a single lower-upper decomposition has to be performed prior to back substitution [17].

In order to evaluate the scattering properties of multilayers of, in general, bianisotropic materials, it is convenient to express the waves on the left (right) of a given interface with respect to an appropriate origin at $-\mathbf{d}_l$ ($\mathbf{d}_r$) from the center. Referred to these new origins, the scattering matrix elements of the interface, for given ω and $\mathbf{q}_\parallel$, become

$$Q_{pp'}^{\mathrm{I}} = S_{pp'}^{++}\exp[i(\mathbf{q}_p^{+(2)}\cdot\mathbf{d}_r + \mathbf{q}_{p'}^{+(1)}\cdot\mathbf{d}_l)],$$
$$Q_{pp'}^{\mathrm{II}} = S_{pp'}^{+-}\exp[i(\mathbf{q}_p^{+(2)}\cdot\mathbf{d}_r - \mathbf{q}_{p'}^{-(2)}\cdot\mathbf{d}_r)],$$
$$Q_{pp'}^{\mathrm{III}} = S_{pp'}^{-+}\exp[-i(\mathbf{q}_p^{-(1)}\cdot\mathbf{d}_l - \mathbf{q}_{p'}^{+(1)}\cdot\mathbf{d}_l)],$$
$$Q_{pp'}^{\mathrm{IV}} = S_{pp'}^{--}\exp[-i(\mathbf{q}_p^{-(1)}\cdot\mathbf{d}_l + \mathbf{q}_{p'}^{-(2)}\cdot\mathbf{d}_r)]. \tag{8}$$

We obtain the reflection and transmission matrices of two consecutive interfaces, n and $n+1$, by combining the matrices of the two interfaces so as to describe interlayer multiple scattering to any order. One can easily prove that the reflection and transmission matrices for the pair of interfaces, denoted by $\mathbf{Q}(n,n+1)$, are

$$\mathbf{Q}^{\mathrm{I}}(n,n+1) = \mathbf{Q}^{\mathrm{I}}(n+1)[\mathbf{I}-\mathbf{Q}^{\mathrm{II}}(n)\mathbf{Q}^{\mathrm{III}}(n+1)]^{-1}\mathbf{Q}^{\mathrm{I}}(n),$$
$$\mathbf{Q}^{\mathrm{II}}(n,n+1) = \mathbf{Q}^{\mathrm{II}}(n+1) + \mathbf{Q}^{\mathrm{I}}(n+1)\mathbf{Q}^{\mathrm{II}}(n) \times[\mathbf{I}-\mathbf{Q}^{\mathrm{III}}(n+1)\mathbf{Q}^{\mathrm{II}}(n)]^{-1}\mathbf{Q}^{\mathrm{IV}}(n+1),$$

$$\mathbf{Q}^{\mathrm{III}}(n,n+1) = \mathbf{Q}^{\mathrm{III}}(n) + \mathbf{Q}^{\mathrm{IV}}(n)\mathbf{Q}^{\mathrm{III}}(n+1) \times [\mathbf{I} - \mathbf{Q}^{\mathrm{II}}(n)\mathbf{Q}^{\mathrm{III}}(n+1)]^{-1}\mathbf{Q}^{\mathrm{I}}(n),$$
$$\mathbf{Q}^{\mathrm{IV}}(n,n+1) = \mathbf{Q}^{\mathrm{IV}}(n)[\mathbf{I} - \mathbf{Q}^{\mathrm{III}}(n+1)\mathbf{Q}^{\mathrm{II}}(n)]^{-1}\mathbf{Q}^{\mathrm{IV}}(n+1). \quad (9)$$

All matrices refer, of course, to the same ω and $\mathbf{q}_\parallel$. We note that the waves on the left [right] of the pair of interfaces are referred to an origin at $-\mathbf{d}_l(n)$ [$\mathbf{d}_r(n+1)$] from the center of the nth [$(n+1)$th] interface. It is obvious that one can repeat the above process to obtain the reflection and transmission matrices of three consecutive interfaces, by combining those of the pair of the first interfaces with those of the third interface; and that we can in similar fashion repeat the process to obtain the scattering matrices of a slab which comprises any finite number of interfaces.

The transmittance $\mathcal{T}$ and reflectivity $\mathcal{R}$ of the slab are defined as the ratio of the transmitted and reflected, respectively, energy flux to the energy flux associated with the incident wave. Integrating the Poynting vector over the $x-y$ plane, on the appropriate side of the slab each time, and taking the time average over a period $T = 2\pi/\omega$, we obtain

$$\mathcal{T} = \frac{\sum_p \left|Q^{\mathrm{I}}_{pp'}\right|^2 \mathrm{Re}\left[\widehat{\mathbf{e}}\left(\mathbf{q}_p^{+(\mathrm{R})}\right) \times \mathbf{h}^\star\left(\mathbf{q}_p^{+(\mathrm{R})}\right)\right]_z}{\mathrm{Re}\left[\widehat{\mathbf{e}}\left(\mathbf{q}_{p'}^{+(\mathrm{L})}\right) \times \mathbf{h}^\star\left(\mathbf{q}_{p'}^{+(\mathrm{L})}\right)\right]_z},$$
$$\mathcal{R} = \frac{-\sum_p \left|Q^{\mathrm{III}}_{pp'}\right|^2 \mathrm{Re}\left[\widehat{\mathbf{e}}\left(\mathbf{q}_p^{-(\mathrm{L})}\right) \times \mathbf{h}^\star\left(\mathbf{q}_p^{-(\mathrm{L})}\right)\right]_z}{\mathrm{Re}\left[\widehat{\mathbf{e}}\left(\mathbf{q}_{p'}^{+(\mathrm{L})}\right) \times \mathbf{h}^\star\left(\mathbf{q}_{p'}^{+(\mathrm{L})}\right)\right]_z}, \quad (10)$$

for a plane EM wave of angular frequency ω, wave vector $\mathbf{q}_{p'}^{+(\mathrm{L})}$, and polarization eigenvectors $\widehat{\mathbf{e}}(\mathbf{q}_{p'}^{+(\mathrm{L})})$, $\mathbf{h}(\mathbf{q}_{p'}^{+(\mathrm{L})})$, incident on the slab from the left, where by (L) and (R) we denote the homogeneous, in general bianisotropic, media which extend to infinity on the left and right sides of the slab, respectively, and $\mathbf{Q}^{\mathrm{I}}$, $\mathbf{Q}^{\mathrm{III}}$ are the corresponding transmission and reflection matrices. If lossy materials are present, the absorbance $\mathcal{A}$ is calculated from energy conservation: $\mathcal{A} = 1 - \mathcal{T} - \mathcal{R}$.

B. Effective-medium approximation

In the present work, we shall be concerned with composite nanoparticles consisting of a dielectric magnetic spherical core of radius S_c coated with a concentric spherical shell of outer radius S. Generally, the optical response of a polycrystalline magnetic material, such as the core material, in the visible and infrared parts of the spectrum is described by a constitutive matrix, defined in Eq. (1), of the form

$$\mathbf{M}_g = \begin{pmatrix} \epsilon_g & -ig & 0 & 0 & 0 & 0 \\ ig & \epsilon_g & 0 & 0 & 0 & 0 \\ 0 & 0 & \epsilon_g & 0 & 0 & 0 \\ 0 & 0 & 0 & 1 & 0 & 0 \\ 0 & 0 & 0 & 0 & 1 & 0 \\ 0 & 0 & 0 & 0 & 0 & 1 \end{pmatrix}, \quad (11)$$

if we consider the magnetization along the z axis. The elements of this matrix are in general complex functions of frequency due to the dissipative and dispersive behavior of the material. We note that the magneto-optical coupling is accounted for by the nondiagonal elements, which change sign upon magnetization reversal and vanish above the Curie temperature. The shell is made of a nonmagnetic plasmonic material characterized by

$$\mathbf{M}_p = \begin{pmatrix} \epsilon_p & 0 & 0 & 0 & 0 & 0 \\ 0 & \epsilon_p & 0 & 0 & 0 & 0 \\ 0 & 0 & \epsilon_p & 0 & 0 & 0 \\ 0 & 0 & 0 & 1 & 0 & 0 \\ 0 & 0 & 0 & 0 & 1 & 0 \\ 0 & 0 & 0 & 0 & 0 & 1 \end{pmatrix}. \quad (12)$$

We shall assume that ϵ_p has the simple yet effective Drude form [20]

$$\epsilon_p = 1 - \frac{\omega_p^2}{\omega(\omega + i\gamma)}, \quad (13)$$

where ω_p is the bulk plasma frequency and γ is the inverse relaxation time of the conduction-band electrons, which accounts for the dissipative losses.

The optical response of an assembly of such magneto-plasmonic nanoparticles, embedded in an optically active homogeneous host medium characterized by a bi-isotropic constitutive matrix of the form

$$\mathbf{M}_h = \begin{pmatrix} \epsilon_h & 0 & 0 & i\gamma_h & 0 & 0 \\ 0 & \epsilon_h & 0 & 0 & i\gamma_h & 0 \\ 0 & 0 & \epsilon_h & 0 & 0 & i\gamma_h \\ -i\gamma_h & 0 & 0 & 1 & 0 & 0 \\ 0 & -i\gamma_h & 0 & 0 & 1 & 0 \\ 0 & 0 & -i\gamma_h & 0 & 0 & 1 \end{pmatrix}, \quad (14)$$

at visible and infrared frequencies, can be described by the effective-medium approximation because the size of the particles is much shorter than the wavelength. An effective constitutive matrix $\mathbf{M}$ can be defined in the spirit of the quasistatic Maxwell-Garnett homogenization method through [21–23]

$$(\mathbf{M} - \mathbf{M}_h)(\mathbf{M} + 2\mathbf{M}_h)^{-1} = f_2(\mathbf{M}_s - \mathbf{M}_h)(\mathbf{M}_s + 2\mathbf{M}_h)^{-1}, \quad (15)$$

where f_2 is the volume filling fraction of the particles and $\mathbf{M}_s$ is an effective constitutive matrix of the core-shell particle given by

$$(\mathbf{M}_s - \mathbf{M}_p)(\mathbf{M}_s + 2\mathbf{M}_p)^{-1} = f_1(\mathbf{M}_g - \mathbf{M}_p)(\mathbf{M}_g + 2\mathbf{M}_p)^{-1}, \quad (16)$$

with $f_1 = (S_c/S)^3$ being the fractional volume of the composite spherical particle occupied by the core. The validity of the Maxwell-Garnett mixing rules is not questionable in our case [24,25].

Equations (15) and (16) are of the form $(\mathbf{X}-\mathbf{A})(\mathbf{X}+2\mathbf{A})^{-1} = f(\mathbf{B}-\mathbf{A})(\mathbf{B}+2\mathbf{A})^{-1}$ and can be readily solved:

$$(\mathbf{X}-\mathbf{A})(\mathbf{X}+2\mathbf{A})^{-1} = f(\mathbf{B}\mathbf{A}^{-1}-1)(\mathbf{B}\mathbf{A}^{-1}+2)^{-1} = f(\mathbf{B}\mathbf{A}^{-1}+2)^{-1}(\mathbf{B}\mathbf{A}^{-1}-1)$$
$$\Rightarrow (\mathbf{B}\mathbf{A}^{-1}+2)(\mathbf{X}-\mathbf{A}) = f(\mathbf{B}\mathbf{A}^{-1}-1)(\mathbf{X}+2\mathbf{A})$$
$$\Rightarrow (\mathbf{B}\mathbf{A}^{-1} + 2\mathbf{A}\mathbf{A}^{-1} - f\mathbf{B}\mathbf{A}^{-1} + f\mathbf{A}\mathbf{A}^{-1})\mathbf{X} = 2(1-f)\mathbf{A} + (1+2f)\mathbf{B}$$
$$\Rightarrow \mathbf{X} = \mathbf{A}[(2+f)\mathbf{A} + (1-f)\mathbf{B}]^{-1}[2(1-f)\mathbf{A} + (1+2f)\mathbf{B}].$$

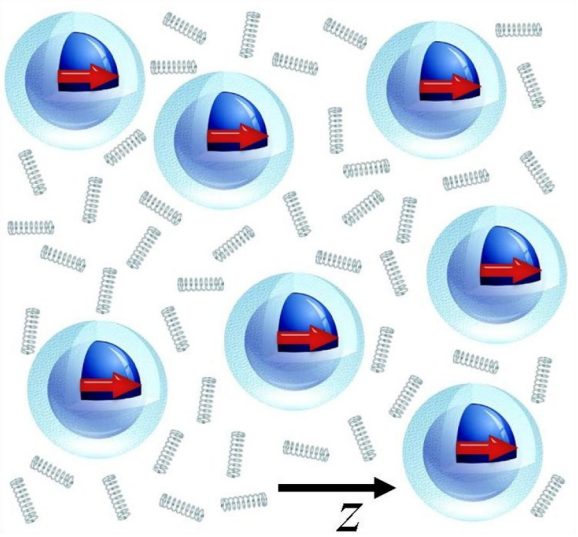

FIG. 1. A schematic view of the metamaterial under consideration: An assembly of composite spherical nanoparticles consisting of a magnetic garnet core ($\epsilon_g = 6.25$, $g = 0.06$), of radius S_c, coated with a lossless plasmonic metal shell, of outer radius S ($S_c/S = 0.8$), embedded in an optically active host matrix ($\epsilon_h = 2.25$, $\gamma_h = 0.1$) with volume filling fraction $f_2 = 0.50$. The direction of magnetization is taken along the z axis.

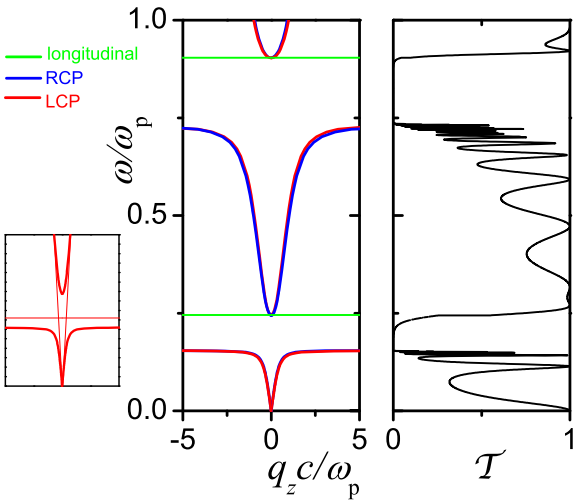

FIG. 2. Left: Photonic band structure of the metamaterial described in Fig. 1 along the magnetization axis. In the inset, we show schematically the hybridization between an extended and a narrow band, of the same symmetry, which leads to the opening of a frequency gap about the crossing point. Right: Corresponding transmission spectrum of a finite slab of thickness $d = 7c/\omega_p$, in air, magnetized perpendicular to its surfaces, for linearly polarized light incident in the direction of magnetization.

III. RESULTS AND DISCUSSION

A. Photonic band structure and transmittance

In the present work, we study the optical properties of a specific realization of the bianisotropic metamaterial described in the previous section, i.e., an assembly of spherical magnetoplasmonic nanoparticles with a core-shell morphology embedded in an optically active host matrix. A schematic view of this metamaterial is depicted in Fig. 1. We assume, for simplicity, that the particles consist of a dispersionless magnetic dielectric core, characterized by a constitutive matrix given by Eq. (11) with $\epsilon_g = 6.25$ and $g = 0.06$, values achievable with magnetic garnets such as bismuth-substituted yttrium-iron garnet [26–28], and a plasmonic shell made of a noble metal material such as silver or gold, described by the Drude relative dielectric function [20] $\epsilon_p = 1 - \omega_p^2/\omega^2$ in Eq. (12), neglecting losses for now. This function naturally introduces ω_p as the frequency unit and c/ω_p as the length unit, which we shall adopt throughout the paper. We note that considering a typical value $\hbar\omega_p = 10$ eV, c/ω_p corresponds to about 20 nm. We further assume that the host medium is characterized by the bi-isotropic constitutive matrix of Eq. (14) with $\epsilon_h = 2.25$ and $\gamma_h = 0.1$. This value of γ_h may seem unusually high for a naturally occurring optically active material; however, there are substances with very strong chirality, an example being helical polymers. For instance, it has been reported that poly-L-lactic acid exhibits a huge optical rotatory power [29], which corresponds to $\gamma_h \sim 10^{-2}$. Moreover, even larger values of the chirality parameter can be achieved with chiral metamaterials [30]. For the relevant geometric parameters, we consider that the ratio of the core to total particle radius, S_c/S, equals 0.8, which corresponds to $f_1 = 0.512$ in Eq. (16), and that the nanoparticles occupy a fractional volume $f_2 = 0.50$ of the composite medium.

The optical response of this medium at visible and infrared frequencies can be described by an effective constitutive matrix $\mathbf{M}$, obtained by Eqs. (15) and (16) because, at wavelengths much longer than the size of the particles and the interparticle spacing, the medium is effectively homogeneous, yet bianisotropic. This type of metamaterial lacks both space-inversion and time-reversal symmetries, but is invariant under proper rotations about the direction of magnetization, which is taken to be along the z axis. Therefore, according to group theory [31], the corresponding dispersion curves of the EM field are rotationally symmetric about the z axis, i.e., they depend on the magnitude but not on the direction of $\mathbf{q}_\parallel$ and

$$\omega_\nu(q_\parallel, q_z) \neq \omega_\nu(q_\parallel, -q_z), \tag{17}$$

where ν is a band index.

In a dielectric, in general bianisotropic, medium, along any direction, the dispersion relation has two extended branches corresponding to the two linearly independent transverse polarization eigenmodes of waves propagating in this medium. However, for the structure under consideration, the effective-medium approximation describes, also, localized dipole plasmons at the two metal-dielectric interfaces [32,33] and, thus, in addition to the extended dispersion curves, six narrow bands (three originating from the cavitylike and three from the particlelike collective dipole plasmon modes) are obtained as well. In general, when two bands of the same symmetry cross each other, level repulsion leads to the opening of a frequency gap about the crossing point. This can be clearly observed in the left-hand diagram of Fig. 2, which depicts the photonic band structure of the metamaterial under study along the direction of magnetization. Two quite sizable gaps appear, indeed, in

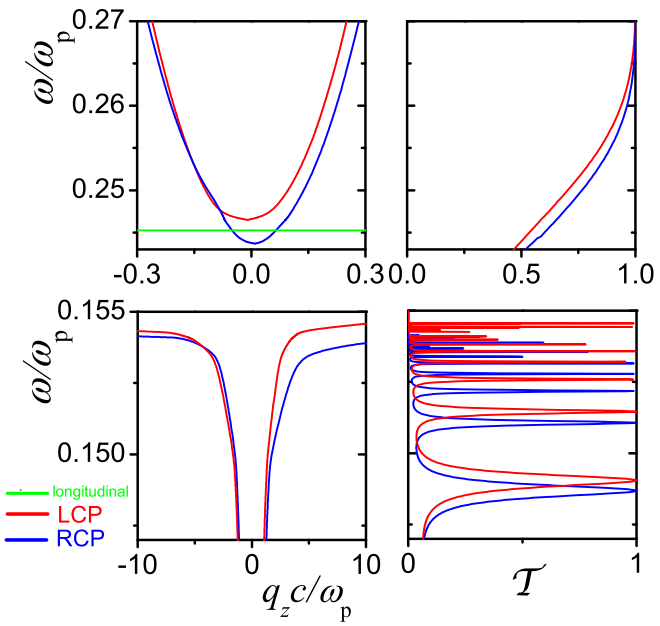

FIG. 3. An enlarged view of Fig. 2 about the lower band gap, with corresponding circular-polarization-resolved transmission spectra.

the frequency regions of the cavity- and particlelike plasmon modes, where the associated flat bands cross the extended dispersion curves. The corresponding transmittance of a finite slab of the given metamaterial is vanishingly small over the range of these so-called hybridization gaps and exhibits Fabry-Pérot oscillations outside the gap regions due to multiple reflections at the surfaces of the slab, as shown in the right-hand diagram of Fig. 2.

The modes of the EM field propagating along the z direction in this metamaterial have the symmetry of the irreducible representations of the C_∞ group, which consists of all proper rotations about the z axis. Since C_∞ is an Abelian group, all of its irreducible representations are one dimensional, thus implying that the corresponding photonic bands are nondegenerate. A dipole vector field (the effective-medium approximation assumes dipole fields) is projected onto the $m = -1, 0$, and 1 irreducible representations of C_∞, which correspond to right-circular polarization (RCP), longitudinal, and left-circular polarization (LCP) modes, with eigenvectors $(\hat{\mathbf{x}} - i\hat{\mathbf{y}})/\sqrt{2}$, $\hat{\mathbf{z}}$, and $(\hat{\mathbf{x}} + i\hat{\mathbf{y}})/\sqrt{2}$, respectively. The two dispersionless (flat) bands, which are clearly visible in the left-hand diagram of Fig. 2, correspond to longitudinal modes stemming from the cavity- and particlelike dipole plasmons and their position is obtained from the condition $\det \mathbf{M} = 0$. The separation between LCP and RCP dispersion curves and the nonreciprocal characteristics of the band diagram, which are not discernible in the scale of Fig. 2, can be clearly observed in Fig. 3, in an enlarged view in the region of the lower-frequency gap. We note that the LCP and RCP bands can be excited by light of the appropriate circular polarization incident normally on a slab of the metamaterial magnetized perpendicular to its surfaces, as shown in Fig. 3, while the longitudinal bands are optically inactive. Along an arbitrary direction, all bands belong, of course, to the trivial representation of the trivial group and are optically active.

Hereafter we shall focus on the spectral region about the lower band gap, which corresponds to visible or near-infrared frequencies and the approximations involved are well justified [21]. We note, however, that the dispersion diagram can be tuned in frequency by varying the composition of the nanoparticles and their concentration in the host medium, which are controlled by the parameters f_1 and f_2, respectively.

B. Nonreciprocal polarization rotation

A linearly polarized light beam, incident normally on a slab of the given metamaterial magnetized perpendicular to its surfaces, of angular frequency ω within the common region of LCP and RCP bands, is decomposed into an LCP and an RCP wave, which propagate through the slab with different phase velocities $\omega/q_{z;1}$ and $\omega/q_{z;2}$, respectively. If the LCP and RCP components of the transmitted wave have the same amplitude, then the transmitted wave is linearly polarized with a polarization direction at an angle

$$\phi = \tfrac{1}{2}(q_{z;2} - q_{z;1})d \tag{18}$$

relative to the polarization direction of the incident wave, where d is the thickness of the slab and positive ϕ means an anticlockwise rotation. As can be seen in the left-hand diagram of Fig. 2, a dispersion curve close to the frequency gap bends and flattens ($d\omega/dq_z \longrightarrow 0$), so that the difference between the wave numbers of the RCP and LCP bands, $q_{z;2} - q_{z;1}$, increases as ω approaches the gap (of course at frequencies where both bands coexist). Therefore, according to Eq. (18), strong polarization azimuth rotation is expected near the frequency gap.

It is worth noting that in the case under consideration, there is no polarization conversion between LCP and RCP waves because these modes span two nondegenerate orthogonal subspaces. This implies that the 2×2 complex transmission matrix of a finite slab, $\mathbf{Q}^{\mathrm{I}}$, in the basis of circularly polarized waves is a diagonal matrix. Its (diagonal) elements, Q_1^{I} and Q_2^{I}, are defined as the ratio of the amplitude of the transmitted to that of the incident LCP and RCP wave, respectively. The transmitted wave is, in general, elliptically polarized with the long axis of the ellipse forming an angle,

$$\phi = \tfrac{1}{2}\big(\arg Q_2^{\mathrm{I}} - \arg Q_1^{\mathrm{I}}\big), \tag{19}$$

with the polarization direction of the incident wave and with ellipticity angle

$$\chi = \arctan \frac{\big|Q_2^{\mathrm{I}}\big| - \big|Q_1^{\mathrm{I}}\big|}{\big|Q_2^{\mathrm{I}}\big| + \big|Q_1^{\mathrm{I}}\big|}. \tag{20}$$

As can be seen in the right- and left-hand diagrams of Fig. 4, the ellipticity angle is relatively small and exhibits small oscillations around zero. We note that a linearly polarized transmitted wave is obtained if $\chi = 0$. In the same diagrams, we also depict the variation of ϕ versus frequency, as calculated from both the dispersion diagram of the infinite metamaterial, by Eq. (18), and the transmitted wave through the given finite slab, using Eq. (19). The results obtained from the transmission calculations oscillate around the smooth curve deduced from the band structure, due to finite-size effects. It can be seen that the polarization azimuth rotation increases as we approach the flat region at the top of the bands, where they have a large horizontal

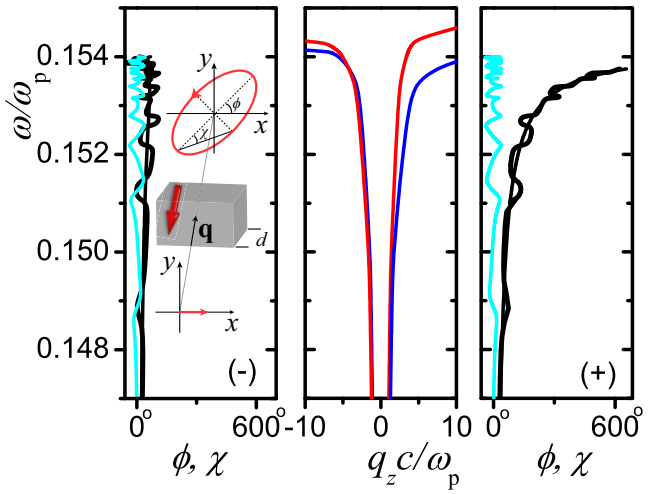

FIG. 4. Middle diagram: An enlarged view of the dispersion diagram of Fig. 2 below the lower band gap. Right- and left-hand diagrams: Ellipticity (bright curves) and azimuth rotation (dark curves) angles of linearly polarized light transmitted through a metamaterial slab of thickness $d = 7c/\omega_p$, in air, magnetized perpendicular to its surfaces, in (+) and opposite to (−) the magnetization direction. A schematic is displayed in the inset.

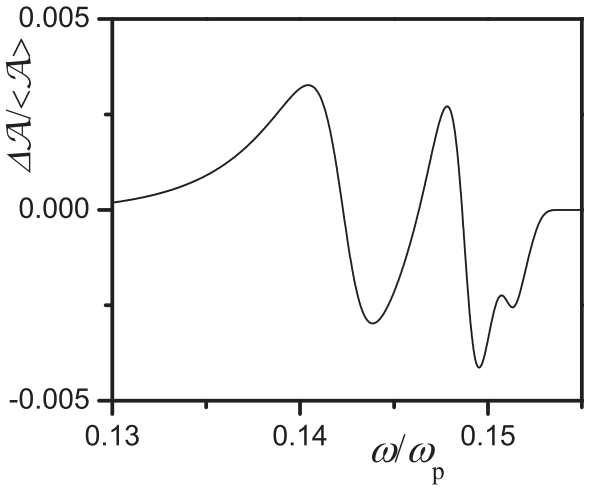

FIG. 5. Magnetochiral dichroism of a slab of the metamaterial under study, of thickness $d = 7c/\omega_p$, magnetized perpendicular to its surfaces, at normal incidence, in the region of the lowest-frequency band. Absorptive losses are taken into account assuming $\epsilon_g = 6.25 + i0.001$ for the magnetic garnet core and $\gamma/\omega_p = 0.002$ for the plasmonic shell.

splitting. In the backward direction, the optical activity induced by the chiral host medium partly counterbalances the magnetic optical activity (Faraday rotation), while in the forward direction chirality and magnetism contribute constructively to yield a strongly enhanced polarization azimuth rotation.

C. Magnetochiral dichroism

Magnetochiral dichroism is a relatively weak, nonreciprocal absorption effect, which can be manifested in a chiral medium magnetized parallel to the direction of propagation of an unpolarized light beam. It is usually defined by the normalized anisotropy factor $\Delta\mathcal{A}/\langle\mathcal{A}\rangle$, with $\Delta\mathcal{A} = \mathcal{A}_+ - \mathcal{A}_-$ and $\langle\mathcal{A}\rangle = (\mathcal{A}_+ + \mathcal{A}_-)/2$, where $\mathcal{A}_\pm$ is the absorbance of unpolarized light incident on a slab of the material in (+) and opposite to (−) the direction of magnetization [34,35]. Unpolarized light can be regarded as an incoherent superposition of LCP and RCP or, in general, of any two orthonormal polarization, light modes. Obviously, in the case under consideration, symmetry implies that unpolarized light is equivalent to linearly polarized light.

In order to study magnetochiral dichroism effects in the metamaterial under consideration, we take into account absorptive losses assuming $\epsilon_g = 6.25 + i0.001$ for the magnetic garnet core and $\gamma/\omega_p = 0.002$ in Eq. (13) for the plasmonic shell. As can be seen in Fig. 5, considerable magnetochiral dichroism, which corresponds to values of the normalized anisotropy factor as large as 0.004, is obtained in the lowest-frequency band. The variations of $\Delta\mathcal{A}/\langle\mathcal{A}\rangle$ follow the Fabry-Pérot oscillations in the region where natural and magnetic optical activity effects are appreciable, but only up to a certain frequency, above which the too-sharp Fabry-Pérot resonances are wiped out by absorption since their lifetime is much longer than the absorption time.

IV. CONCLUSION

In summary, we proposed and analyzed a generic type of nonreciprocal, frequency-tunable optical metamaterial, which consists of metal-coated dielectric spherical nanoparticles immersed in an optically active host medium. This metamaterial, which can be synthesized in the laboratory (see Ref. [36] and references therein), combines gyrotropy, plasmonic resonances, and chirality, and exhibits some remarkable properties, such as nonreciprocal polarization azimuth rotation and magnetochiral dichroism, which stem from the simultaneous lack of time-reversal and space-inversion symmetries and are enhanced by collective resonant plasmon modes. We calculated the optical properties of this medium, using a six-vector formulation of Maxwell equations and a two-step homogenization approach based on a proper generalization of Maxwell-Garnett effective-medium theory, and provided a consistent interpretation of the underlying physics.

ACKNOWLEDGMENT

A.C. acknowledges support by the Greek State Scholarships Foundation (IKY) through the program "Strengthening Post Doctoral Research" (Contract No. 2016-050-0503-7197).

[1] V. I. Belotelov, I. A. Akimov, M. Pohl, V. A. Kotov, S. Kasture, A. S. Vengurlekar, A. V. Gopal, D. R. Yakovlev, A. K. Zvezdin, and M. Bayer, Nat. Nanotechnol. **6**, 370 (2011).

[2] M. Liu and X. Zhang, Nat. Photon. **7**, 429 (2013).

[3] G. Armelles, A. Cebollada, A. García-Martín, and M. U. González, Adv. Opt. Mater. **1**, 10 (2013).

[4] D. Floess, T. Weiss, S. Tikhodeev, and H. Giessen, Phys. Rev. Lett. **117**, 063901 (2016).
[5] E. Almpanis, P. A. Pantazopoulos, N. Papanikolaou, V. Yannopapas, and N. Stefanou, J. Opt. Soc. Am. B **33**, 2609 (2016).
[6] A. Figotin and I. Vitebsky, Phys. Rev. E **63**, 066609 (2001).
[7] Z. Yu, G. Veronis, Z. Wang, and S. Fan, Phys. Rev. Lett. **100**, 023902 (2008).
[8] Y. Hadad and B. Z. Steinberg, Phys. Rev. Lett. **105**, 233904 (2010).
[9] A. B. Khanikaev, S. H. Mousavi, G. Shvets, and Y. S. Kivshar, Phys. Rev. Lett. **105**, 126804 (2010).
[10] A. Christofi and N. Stefanou, Int. J. Mod. Phys. B **28**, 1441012 (2014).
[11] F. Jonsson and C. Flytzanis, Phys. Rev. Lett. **97**, 193903 (2006).
[12] C. He, M. H. Lu, R. C. Win, T. Fan, and Y. F. Chen, J. Appl. Phys. **108**, 073103 (2010).
[13] A. Christofi, N. Stefanou, and G. Gantzounis, Phys. Rev. B **83**, 245126 (2011).
[14] U. Gubler and C. Bosshard, Nat. Mater. **1**, 209 (2002).
[15] J. B. Pendry, Science **306**, 1353 (2004).
[16] X. L. Zhou, Prog. Electromagn. Res. **64**, 117 (2006).
[17] W. H. Press, S. A. Teukolsky, W. T. Vetterling, and B. P. Flannery, *Numerical Recipes: The Art of Scientific Computing* (Cambridge University, Cambridge, 2007).
[18] F. Tisseur and K. Meerbergen, SIAM Rev. **43**, 235 (2001).
[19] S. Hammarling, C. J. Munro, and F. Tisseur, ACM Trans. Math. Softw. **39**, 1 (2013).
[20] N. W. Ashcroft and N. D. Mermin, *Solid State Physics* (Saunders, New York, 1976).
[21] P. Varytis, P. A. Pantazopoulos, and N. Stefanou, Phys. Rev. B **93**, 214423 (2016).
[22] A. H. Sihvola and O. P. M. Pekonen, J. Phys. D: Appl. Phys. **29**, 514 (1996).
[23] A. Sihvola and F. Olyslager, Radio Sci. **31**, 1399 (1996).
[24] B. Shanker, J. Phys. D: Appl. Phys. **30**, 289 (1997).
[25] A. H. Sihvola and O. P. M. Pekonen, J. Phys. D: Appl. Phys. **30**, 291 (1997).
[26] V. Doormann, J. P. Krumme, and H. Lenz, J. Appl. Phys. **68**, 3544 (1990).
[27] S. M. Drezdzon and T. Yoshie, Opt. Express **17**, 9276 (2009).
[28] K. Fang, Z. Yu, V. Liu, and S. Fan, Opt. Lett. **36**, 4254 (2011).
[29] Y. Tajitsu, R. Hosoya, T. Maruyama, M. Aoki, Y. Shikinami, M. Date, and E. Fukada, J. Mater. Sci. Lett. **18**, 1785 (1999).
[30] S. S. Oh and O. Hess, Nano Converg. **2**, 24 (2015).
[31] J. F. Cornwell, *Group Theory in Physics* (Academic, London, 1984), Vols. I and II.
[32] P. Varytis, N. Stefanou, A. Christofi, and N. Papanikolaou, J. Opt. Soc. Am. B **32**, 1063 (2015).
[33] P. Varytis and N. Stefanou, Opt. Commun. **360**, 40 (2016).
[34] A. Christofi and N. Stefanou, Opt. Lett. **38**, 4629 (2013).
[35] V. Yannopapas and A. G. Vanakaras, ACS Photon. **2**, 1030 (2015).
[36] R. Y. Hong, Y. M. Wang, L. S. Wang, Y. J. Wu, and H. Z. Lin, in *Yttrium: Compounds, Production and Applications*, edited by B. D. Volkerts (Nova Science, New York, 2011), pp. 127–154.